NANOMETRIC ALUMINIUM POWDER INFLUENCE ON THE DETONATION EFFICIENCY OF EXPLOSIVES

A. Lefrancois[#], G. Baudin[#], C. Le Gallic[#]
and
P.Boyce*, J-P Coudoing*

[#]French Ministry of Defense DGA/DCE/CEG
Centre d'Etudes de Gramat (CEG)
46500 Gramat - France

*French Ministry of Defense DGA/DCE/CTSN
Centre Techinque des Sytèmes Naval (CTSN/VN/TCO), BP 28
83800 Toulon - FRANCE

The detonation characteristics and ballistic efficiency of RDX-AP-Al-WAX high explosives (HE) containing 5 μm and 100 nm aluminum with several oxygen balances have been investigated. Cylinder tests have been performed with detonation velocity, front shape and thermal emission spectra measurements. A preliminary study of heat conduction at the interface LiF-RP and of radiation transfer inside RP has been performed prior emission spectra analysis and temperature determination. Experimental detonation velocity-wave curvature relationships are compared to CHEETAH 2.0 calculation and numerical 2-phases modeling. Decreasing in aluminum particles diameter doesn't affect significantly the detonation velocity-wave curvature relationship and lead to lower cylinder expansion velocities. However, higher detonation products temperatures are obtained for nanometric aluminum.

In addition, blast and underwater efficiency are studied. HE previously investigated are tested and compared to TNT reference data, using cylindrical charges of 12 kg detonated on the ground or underwater. Decreasing the aluminum diameter enhances significantly the reflected pressure and impulse, the underwater impulse and the bubble effect.

INTRODUCTION

Use of aluminum particles in high explosives (HE) is well known to improve their efficiency. The influence of different parameters such as the weight contents, the particle size, the particle distribution and the particle morphology has been the scope of many experimental and numerical studies.

Exploratory studies[1-3] highlights the potential interest of reducing the aluminum powder to nanometric scale through particle size distribution measurements and Differential Scanning Calorimetry (DSC):
- increasing in the powder specific surface area, and so in the heat transfer,
- increasing in the oxidation rate.

If this prediction has been shown in the field of propulsion with, in particular the increase of the combustion velocity, this is not so obvious for high explosives.

Aluminum nanoparticles (Argonide "Alex" powders and powders manufactured in France by CNRS) addition into nitromethane and TNT have been previously investigated at CEG (G. Baudin et al[1] and A. Lefrançois et al[4]) without real improvement in detonation characteristics and ballistics. The reasons was attributed to the very small reaction zone of these HE. Only a small increase in the side-on impulse has been obtained in aerial explosion experiments for TNT-Al based HE, comparing to aluminum particles diameter of a few microns. Other

authors intensively studied addition of aluminum[5], and highlights an increasing in detonation velocity for ADN-Alex based HE.

Nanometric Al powders was still expected to give a potential interest in highly non-ideal HE to release oxidation energy in their large subsonic reaction zone that sustains the detonation propagation, and in their very slow detonation product expansion.

This paper proposes a review of results obtained for highly non-ideal HE containing RDX, AP, Al and wax binder. HE investigated are the following:

TABLE 1 - HE INVESTIGATED

HE	*Tritonal*	*G258N*	*G258M*	*G258L*
Density (g/cm^3)	1.60	1.664	1.654	1.659
Additives	Al	100nm Al	5µm Al	5µm LiF
Composition (wt. %)	TNT/Al 80/20	RDX/AP/Additives/ wax 50/24/12/14		

HE	*G111N*	*G111M*	*G111L*
Density (g/cm^3)	1.805	1.793	1.789
Additives	100nm Al	5µm Al	5µm LiF
Composition (wt. %)	RDX/AP/Additives/ wax 20/43/25/12		

Their sensitivity in fall-hammer and friction test have been investigated by A. Lefrançois et al.[4].

DETONATION VELOCITY AND WAVE CURVATURE

Experimental method

H.E. steady detonation velocity and shape of the detonation front are measured inside 3" test cylinder experiments using piezoelectric pins (fig. 1). The function that we considered to fit the shape $z_F(r)$ of the detonation front is the following $z = z_0 + A\left(e^{-b(r-r_0)} + e^{b(r-r_0)} - 2\right)$. It allows the fitting for a large variety of H.E. using only a few points along the detonation front (9-11 points). Then, the radius of curvature R_C, the curvature $\kappa=1/R_C$ and the normal detonation velocity D_n to the front can be easily determine for a given diameter of the HE stick.

The D_n-κ curve is a detonation characteristic for a given HE stick diameter. If the subsonic HE reaction zone is very small compared to the radius of curvature (i.e. the stick diameter), this curve is a detonation characteristic independent of stick diameter which can be given by the Bdzil and Stewart "Detonation Shock Dynamic" model[6] (DSD). This model is an extension of the Wood & Kirkwood model[7] (WK) out of axis, assuming a quasi-1D and quasi-steady flow toward the normal direction to the front.

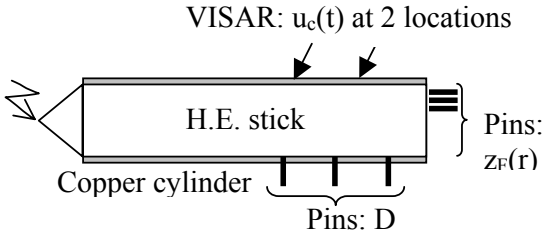

FIGURE 1 - 3" TEST-CYLINDER CONFIGURATION.

Experimental and numerical results

Figures 2 and 3 show the experimental velocity D_n-κ curves obtained for G111M, G111N, G258L, G258M and G258N. Theoretical lines are determined using the WK model in the thermochemical code Cheetah 2.0[8], and using a multiphase model developed for CHNO-AP-Al HE by A. Chinnayya et al[9].

In both two models, the concentrations of RDX, AP, Al and WAX are kinetically controlled by a pressure-dependant rate law $\dot{\lambda} = A(1-\lambda)^a (P/P_0)^b$ describing the surface controlled reactions.

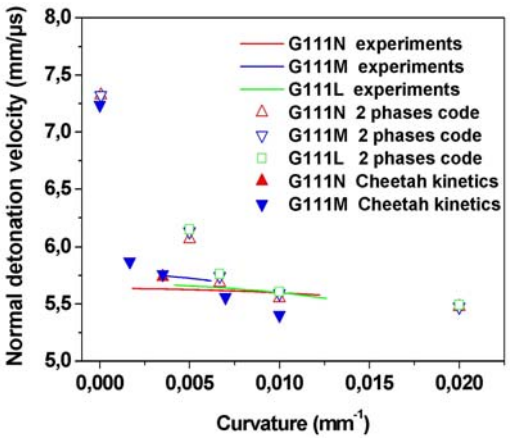

FIGURE 2 - D_n - κ CURVES FOR G111, 3" TEST CYLINDER.

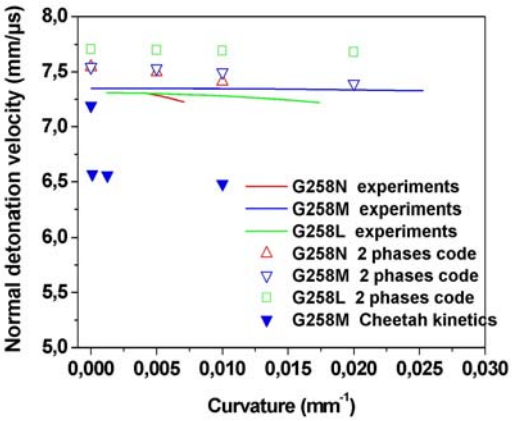

FIGURE 3 - D_n - κ CURVES FOR G258, 3" TEST CYLINDER.

Cheetah thermodynamically controls the other chemical species; their concentrations are kept at equilibrium with the evolving mix of species using the BKW E.O.S. for the gaseous phase and a modified Murnaghan E.O.S. for the condensed phases, including a 3-phase carbon description.

In multi-phase model, the two phases pressures and particle velocities are assumed in equilibrium. Each phase has its own temperature without heat exchange. The diameters d_0 of grains and particles are taking into account using a spherical grain burning model with $\dot{d} = cste$. In this case, $A = 6\dot{d}/d_0$ and $\dot{d}$ has been identified from PBXN-111 D_n-κ data.

The agreement between experiment and theory is good for G111M-N HE for both two models at curvature greater than 0.005. For lower curvature, the detonation velocity drops rapidly from its ideal limit at ∞ values of κ. Discrepancies between experiment and theory are obtained for G258M-N for both two models: CHEETAH kinetics led to under-estimating detonation velocities and the multiphase model over-estimates their values.

If the multiphase model doesn't lead to quantitative prediction, it gives qualitative influence of the aluminum particles diameter and of non-reactive LiF particles in the reaction zone. LiF and Al having very closed thermodynamic properties, LiF has been simulated by considering non-reactive aluminum. It seems that the discrepancies between experiment and theory are due for both kinetics and thermochemical equilibrium. Both experiments and simulations show that a decreasing in aluminum particles diameter doesn't change significantly the D_n-κ characteristic.

For H.E. containing 100 nm aluminum, a non negligible initial fraction of Al_2O_3 is present: a 3 nm Al_2O_3 thickness observed at the surface of Al particles[1] led to a 18.7% weight contents for G111N and 9.0% for G258N. CHEETAH thermochemical simulations taking into account this Al_2O_3 fraction, and assuming both CJ model and Al non-oxidation, led to respectively 500 m/s and 120 m/s decreasing in detonation velocity for G111N and G258N compared to calculations without Al_2O_3. It will be important to take into account this initial Al_2O_3 weight fraction in future predictions.

BALLISTICS

Experimental set up

The experimental set up is represented figure 1. The copper liner velocity of the cylinder test is measured with a good accuracy using two VISAR set up at two different locations

from the back of the cylinder. The registration time allows a precisely determination of the HE driven shock loading phase of copper cylinder and the long reaction zone influence for RDX-AP-Al-wax based HE.

Experimental results

The two VISAR measurements don't show any difference for each cylinder test, confirming that detonation is steady. The cylinder velocities of G111 and G258 compositions are presented figure 4.

HE G258M (5µm Al) exhibits the best ballistic efficiency. Compared to G258N (Al 100 nm), the velocity gap is about 10 % at 10 µs. G258L velocity is between G258N and G258M ones. For G111N, G111M and G111L HE, the cylinder expansion velocities are quite similar.

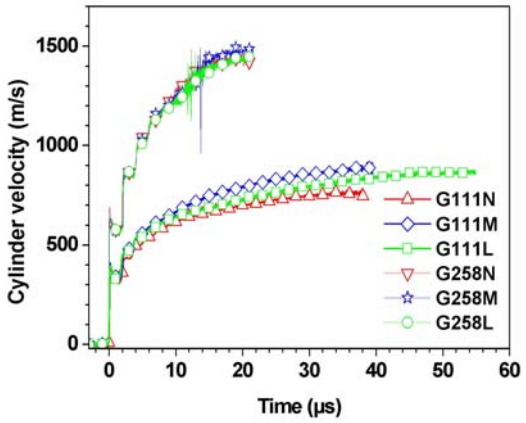

FIGURE 4 - CYLINDER TEST VELOCITIES MEASURED USING VISAR.

Nanometric aluminum additive in RDX-AP-Al-wax HE slightly decrease their ballistics for high RDX weight percent and has no influence for lower RDX weight percent. We expect that this behavior is mainly due to the presence of initial alumina layer at the surface of the particles.

THERMAL CHARACTERISTICS

Experimental method

Radiative properties of the reaction products of G111 and G258 HE compositions are measured using a six wavelength optical pyrometer[10] in the range 500-1500 nm. This apparatus allows the measurement of time resolved emission spectra of a finite layer of HE reaction products (RP) along a single line of sight and through a LiF window glued to HE. The six wavelength are 500±40, 650±50, 850±30, 1100±30, 1270±50 and 1510±50 nm. Calibration of the system, including the LiF window, is performed using a blackbody, up to 3300 K. The system of flux collection is represented on figure 5.

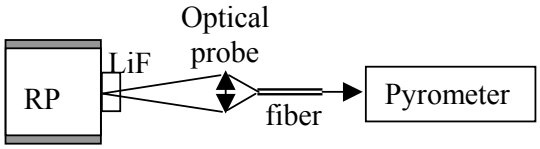

FIGURE 5 - SYSTEM OF FLUX COLLECTION.

Experimental results

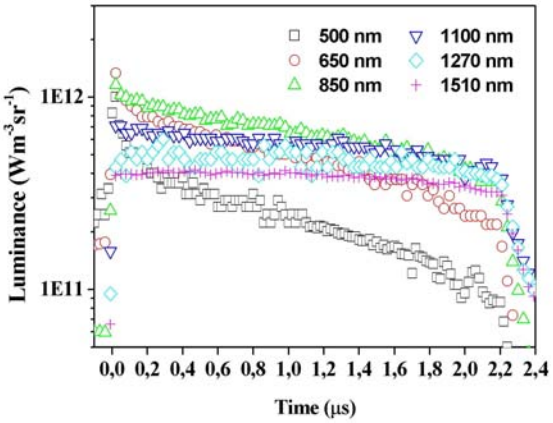

FIGURE 6 - TIME RESOLVED EMISSION SPECTRA OF G258N DP.

Typical time resolved emission spectra are shown on figure 6. At t=0 µs, the detonation front enters the LiF windows. For positive times, the thermal radiation seems to be the predominant mode of emission and radiation transfer inside RP. At the interface LiF-RP, conduction heat transfer leads to a temperature gradient inside a small thickness of DP and LiF[11]. Non thermal radiation can

also occur at the shock entrance inside the LiF window, due to energy transfer from shock to LiF at the molecular level[12]. These two phenomena led to analyze HE DP spectra 1 μs after the shock entrance inside the LiF window.

The analysis of emission spectra needs a preliminary study of heat conduction at the interface LiF-RP and of radiation transfer inside RP.

Effect of heat conduction

In the general case, the heat conduction problem at LiF-RP interface requires numerical simulation. Analytical solution exists for only uniform or linear temperature profiles inside the two materials. Radiation transfer occurs on a small thickness of RP: several microns up to 500 microns, dependant on the wavelength (see later in this paper). Thus an initial uniform temperature profile inside LiF and RP in the vicinity of the interface can been assumed: only a 15 K/mm temperature gradient comparing to 3100 K at interface has been calculated using a 1D lagrangian hydrodynamic code. In such consideration, the analytical solution of conduction heat transfer at DP-LiF interface leads to temperature gradient inside a DP thickness equal to $\delta = 4\sqrt{\frac{k}{\rho C_P}t}$. Assuming that DP are mainly composed of N_2, H_2O, CO, CO_2, CH_4, C, Al and Al_2O_3, a magnitude of thermal conductivity k is ~10^{-3} W/cm.K at ambient pressure and ambient temperature. In an other hand, Cheetah calculations led to ρC_P ~ 5 J/cm^3.K. From these data, temperature gradient holds inside a 0.5 μm DP thickness, 1 μs after shock entrance inside the LiF window. Comparing to the radiation optical thickness (several μm up to 500 μm), this thermal conduction thickness can be neglected.

DP radiation transfer

The governing equations for radiation heat transfer (RTE) are derived by making a radiation energy balance on a differential volume element along a single line of sight[13]. The assumptions of randomness, homogeneity and continuity are implied in this formulation. A dispersed medium may be considered homogeneous if particles diameters are small compared to the medium thickness[14]. RTE is an integro-differential equation that may be written in terms of the spectral intensity I_λ of radiation propagating in a direction $\vec{s}$:

$$\frac{dI_\lambda(\vec{s})}{ds} = -(\sigma_\lambda + \kappa_\lambda) I_\lambda(\vec{s}) + \kappa_\lambda I_{0\lambda} + \frac{\sigma_\lambda}{4\pi}\int_{4\pi} I_\lambda(\vec{s}') P_\lambda(\vec{s}' \to \vec{s}) ds'$$

where σ_λ and κ_λ are the scattering and absorption spectral coefficients, and $I_{0\lambda}$ the Planck's blackbody function. The spectral scattering phase function $P_\lambda(\vec{s}' \to \vec{s})$ is the probability that the radiation propagating in the direction s' is scattered in the direction s, normalized such that $\frac{1}{4\pi}\int_{4\pi} P_\lambda(\vec{s}' \to \vec{s}) ds' = 1$.

The scattering and absorption coefficients, and the scattering phase function may be calculated assuming independent scattering or by modeling the dependant effects. A well known independent scattering model is the full Mie scattering theory assuming spherical particles. It is useful to examine some limiting regions of this model where simpler analytic model can be applied.

These regions are defined by the magnitude of the particle size parameter $x=\pi d/\lambda$, d being the particles diameter and λ the wavelength, the complex index m=n-ik and the volume fraction α_v of particles. The parameter x and the volume fraction α_v determine independent or dependant scattering of particles. Independent scattering falls into three well known limit regimes:

- When the particles are much smaller than the wavelength ($x<<1$) with a moderate refractive index n, the limiting solution of

Mie theory is known as Rayleigh scattering.

- Near-dielectric spheres with k≈0 and with a refractive index n closed to 1 (|m-1|<<1) has negligible reflectivity and the light pass into spheres unattenuated and unrefracted; if x|m-1|<<1 holds for arbitrary x, the light will exit the sphere again unattenuated, and the limiting solution of Mie theory is known as Rayleigh-Gans scattering.
- When the particle is large comparing to the wavelength (x>>1) and the refractive index change to surrounding verifies x|m-1|<<1, geometric optics and diffraction theory can be used.

The validity of applying these models is an issue of a careful analysis, case-by-case, of scattering particularities inside the studied medium. Applying to HE RP needs to extrapolate 1atm gas and particulate thermo-optic behavior, also scattering considerations, up to 20 GPa and 3000 K conditions. Volume fraction of carbon and Al, 10 % C - 21% Al for G111 DP and 15% C - 10% Al for G258 DP, calculated at inert Al CJ states (Cheetah 2.0), indicates independent scattering inside the HE reaction zone.

In detonation products, carbon particles size is very small (a few nm[15]) and are much smaller than the wavelength in the visible and near infrared range ($x \approx 10^{-2}$). Their refractive index is moderate (e.g. m=2.2-1.12i for soot in combustion application[13]). Such particles fall into the Rayleigh scattering regime.

Alex powders are mainly composed of very small particles (d<100 nm) which fall into the Rayleigh regime ($x_{max} \approx 0.6$ and m=4.46-31.5i[13]) and of a few particles with d ≈ 1μm which falls into the geometric optics and diffraction theory. Rayleigh scattering associated with a geometric optics and diffraction theory seems to be a good way to model such particles, by neglecting the effects of a few number of particles that fall into the full Mie regime.

5 μm aluminum particles are much greater than the wavelength in the visible and near infrared range (10<x<30) and fall into a geometric optics and diffraction regime. Because of their high reflectivity in all directions, large aluminum particles tend to be almost isotropic scatters[13], which simplifies the scattering modeling ($P_\lambda(\vec{s}' \to \vec{s}) = 1$). However, aluminum has a dip in reflectivity centered at λ~0.8 μm due to bond electron transitions at ambiant pressure. The normal spectral reflectivity lies between 0.9 and 0.93 for 0.1<λ<0.7 μm and between 0.95 and 0.98 for 1<λ<2 μm.

Presence of a thin oxide layer on aluminum (up to 100 Angstrom) appreciably increases aluminum emissivity for wavelength less than 1.5 μm[13]. It is not true for thick oxide layers; aluminum with a thick layer of alumina (Al_2O_3) doesn't display the typical trends of metals but exhibit the behavior of the dielectric alumina, e.g. the Rayleigh-Gans regime for diameter smaller than 100 nm (m=1.75+0i[13]). However, it is often assume that alumina is dispersed into the gaseous detonation products as atomize phase (pseudo-gas phase), because its dilatation 14 times smaller than Al one.

In Rayleigh regime, e.g. for carbon and aluminum size smaller than 100 nm, scattering has certain similarities to classical absorption. For a DP layer at uniform temperature, RTE equation falls into the form $I_\lambda = I_{0\lambda}(T)\left(1 - e^{-\kappa_\lambda s}\right)$ with $\kappa_\lambda = \frac{\alpha_v C_0}{\lambda}$ and $C_0 = 6\pi\Im\left\{\frac{m^2 - 1}{m^2 + 2}\right\}$.

In geometric optics and diffusion theory, for isotropic scatters, e.g. aluminum size greater than 1 μm, scattering has also certain similarities to classical absorption, with $\kappa_\lambda = \frac{3}{2}\frac{\alpha_v}{d}\left(1 - \rho_\lambda^{'}\right)$, $\rho_\lambda^{'}$ being the spectral

hemispherical reflectivity, for clouds of uniform size spherical particles.

Finally a model for the mix of species is

$$\kappa_\lambda = \sum_i \frac{\alpha_{vi} C_{0i}}{\lambda} + \sum_j \frac{3}{2} \frac{\alpha_{vj}}{di} \left(1 - \rho'_{\lambda j}\right) + \kappa_{\lambda g} \cdot$$

i is carbon, Al_2O_3 and Al particles of size smaller than 100 nm, j is Al particles of size greater than 1 μm and $\kappa_{\lambda g}$ is the absorption coefficient of the gaseous phase. Variations of hemispherical reflectivity and refractive index versus the wavelength are small on large bands. Thus, out of gas emission lines, the model falls into the form $\kappa_\lambda = \frac{A}{\lambda} + B$.

Because of dip in reflectivity of aluminum, the magnitude of B will be different in the two wavelength range $0.1<\lambda<0.8$ μm and $0.8<\lambda<2$ μm.

The DP gas emission bands in the visible and near IR are mainly H_2O spectral lines. The wavelength of the pyrometer are out of these lines except for the wavelength 1100 nm. Because of the difficulty to model the gas emission bands in detonation pressure and temperature, a careful analysis of spectra and elimination of wavelength close to gas lines at ambient pressure is necessary before fitting I_λ with our κ_λ model.

A first theoretical evaluation of κ_λ for clouds of uniform size spherical particles shows that

- $\kappa_\lambda = \frac{5.023\alpha_v}{\lambda}$ for carbon,
- $\kappa_\lambda = \frac{0.016\alpha_v}{\lambda}$ for nanometric Al,
- $\kappa_\lambda \approx 0$, for nanometric Al2O3,
- $\kappa_\lambda \approx 0.025\alpha_v$ μm^{-1} in the range $0.1<\lambda<0.7$ μm and $\kappa_\lambda \approx 0.011\alpha_v$ μm^{-1} in the range $1<\lambda<2$ μm for 5μm Al.

A calculation of the optical thickness corresponding to 10% of radiation energy transmitted, leads to 2 μm for carbon and 350 μm for aluminum particles diameter of 5 μm. Contributions of atomize Al_2O_3 and nanometric aluminum to Rayleigh scattering are very small.

Carbon are usually assume in thermal equilibrium with the gas phase, but it is not necessarily true for aluminum and alumina in the first microsecond of release wave. From the previous analysis of radiation transfer, we can expect that gaseous DP temperature will be determined for HE containing nanometric aluminum, because of negligible contribution of Al_2O_3 and nano aluminum out of gas rays. On the contrary, the aluminum temperature will be determined for HE containing 5μm aluminum particles.

Analysis of experimental results and temperature calculation

The figure 7 exhibits a typical example of spectrum fitting for G258N containing nm aluminum particles using our radiation model. The temperatures and κ_λ parameters obtained are given in table 2 for all HE investigated.

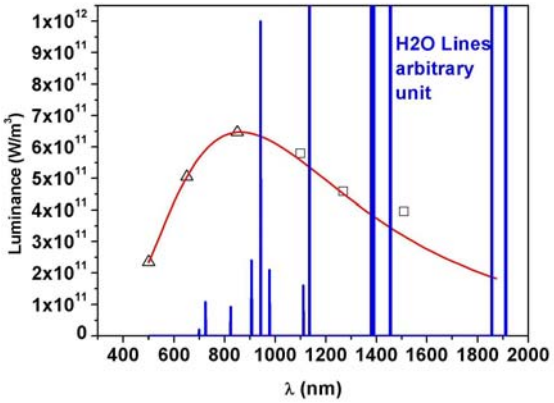

FIGURE 7 - TYPICAL EXAMPLE OF SPECTRUM FITTING FOR G258N.

Both G111 and G258 HE exhibit experimental and theoretical trends in good agreement for the variation of B parameter versus aluminum particle diameter. It is surprising that the carbon A theoretical value ($5.02\alpha_v$=0.753) is close to the fitting one (0.744) for G258N DP.

TABLE 2 - TEMPERATURES AND κ_λ PARAMETERS OBTAINED FOR G111 AND G258 HE

HE	*T (K)*	*A*	*B (μm^{-1})*
G111N	3490 ± 137	0 ± 0.003	0.081 ± --
G111M	2582 ± 54	0 ± 0.004	0.244 ± 0.031
G258N	3037 ± --	0.744 ± --	0.124 ± --
G258M	2947 ± --	1.018 ± --	2.720 ± --
G258L	2453 ± 25	Grey body fitting	

The small contribution of Rayleigh scattering obtain for G111 HE seems to highlight a very low volume fraction of carbon in DP. For G111 HE, the temperature obtained is probably aluminum temperature. It is not so clear for G258 HE: G258N DP temperature seems to be the gas temperature whereas we can not conclude for G258M DP. The low temperature obtained for G258L (2453 K comparing to ~ 3000 K with aluminum) seems to be the gas temperature. This result is in favor of thermal non-equilibrium aluminum-gas phase mix.

It is clear that higher temperatures are obtained for "Alex" nano-particles based compositions. A gap of ~ 1000 K is obtained for G111 HE and ~ 100 K for G258 HE comparing to μm Al, taking into account the previous radiation transfer model.

BLAST CHARACTERISTICS

Experimental set-up

Blast experiments have been performed using cylindrical charges detonated on ground surface. The configuration is presented figure 8. A reinforced concrete platform is built for an ideal surface reflection. We try also to reduce the sensor vibration by shock absorber media and splitting off the measurement platform from the cylindrical charge support. For all the tests, pressure gauges settled at 6 m from the charge are nevertheless very noisy.

The pressure gauges are PCB piezoelectric with integrated amplifier, the signals are recorded by a Nicolet acquisition card system. The side-on pressure gauges are implanted for several radial lines at the distances 1.65 m to 6 m along three axis, and along only two axis from 9 m up to 15 m. Only the positive phase of the side-on signals is determined in these tests, because of a reflected wall positioned at an optimized stand-off distance from the charge. Three reflected pressure measurements are performed on the wall. High-speed camera and speed video camera (about 1000 frames/s) are also implanted to show the fire ball evolution and the blast effects.

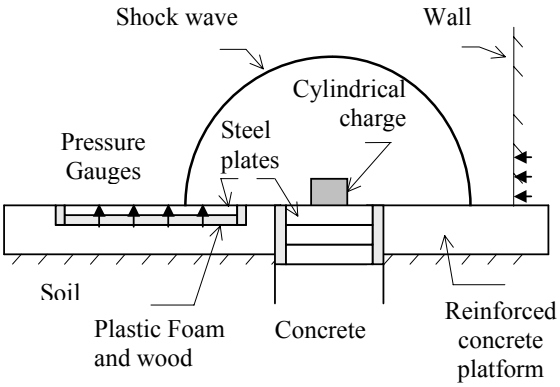

FIGURE 8 - EXPERIMENTAL SET-UP FOR CYLINDRICAL CHARGE TESTS (SIDE VIEW)

Four high explosives are compared in this paper : Tritonal as reference and the three high explosives G111, see table 1. The same cylindrical booster is used for the whole tests, with a 500 g weight and a HMX/Viton 95/5 composition. Because the charge detonates on the ground, the initiation train occurs with the following elements : a detonator, a detonating cord, a small cylindrical booster and a large cylindrical booster. The direct comparison of the blast parameters is made by the volume : 7 liters.

Experimental Results

The side-on pressure and impulse versus distance are presented figures 9 and 10.

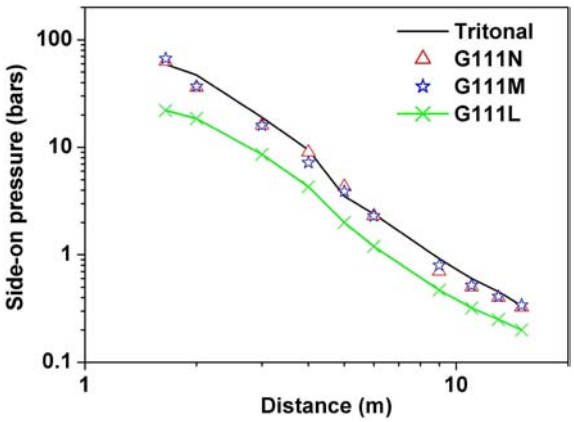

FIGURE 9 - SIDE-ON PRESSURE VERSUS DISTANCE

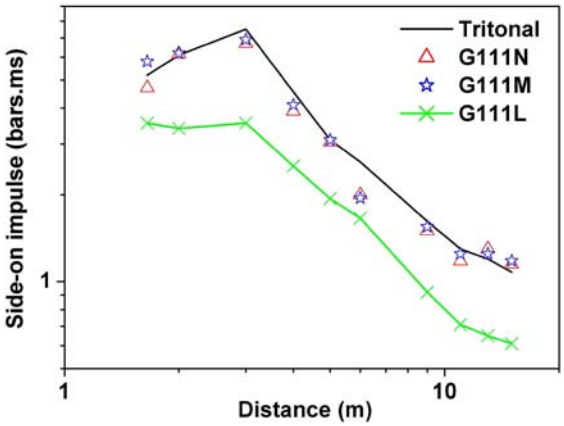

FIGURE 10 - SIDE-ON PRESSURE VERSUS DISTANCE

The composition G111L without aluminum content shows the lowest pressure and impulse versus distance. Tritonal has the highest results of the four compositions, except in the near field (at the distance of 1.65 meter). These blast parameters are doubled compared to G111L.

The composition G111M (5 µm aluminum) has the best blast parameters in the near field (at 1.65 meter), 6% in pressure and 23 % in impulse compared to the composition G111N (100 nm Al).

Except in the near field, the compositions G111N and G111M give similar pressure and impulse. The maximum difference is less than 14 % in pressure (except at 4 meter), and 5 % in impulse. The results of G111N and G111M are below Tritonal. The maximum difference with Tritonal is 27 % in pressure (measured at the distance of 2 meter), and 14 % in impulse (measured at the distance of 4 meter).

Reflected blast pressure and impulse are presented table 3, measured at 4 meter. The same results as the side-on blast parameters are obtained for G111L and Tritonal. The composition G111N gives very surprising results. The reflected blast parameters are higher than the composition G111M, 82% in pressure and 16 % in impulse. The pressure of G111N is equal to Tritonal. And the impulse is 14 % below Tritonal.

TABLE 3 - REFLECTED BLAST PARAMETERS AT 4 M

HE	*Trito-nal*	*G111N*	*G111M*	*G111L*
Reflected pressure	40 bars	40	22	19.3
Reflected impulse	18.2 bars.ms	16	13.75	10.4

UNDERWATER EXPERIMENTS

Experimental set-up

A serie of free-field underwater detonation has been performed. The objective is to quantify and classify the performance of the compositions G111N, G111L when fired underwater. These trials were performed at CTSN site in the Mediterranean sea close to Toulon.

The experimental set-up is shown figure 11. The cylindrical charges are suspended at mid-depth in free water with buoys at roughly 10 meters depth with the seabed being at 20 meters to minimize the effects of surface and bottom reflections. The shock waves and bubble pulses are measured by 6 tourmaline pressure gauges fixed on a vertical cable below the charge, and 3 additional pressure gauges deployed 4.5 meters away on a second parallel vertical line.

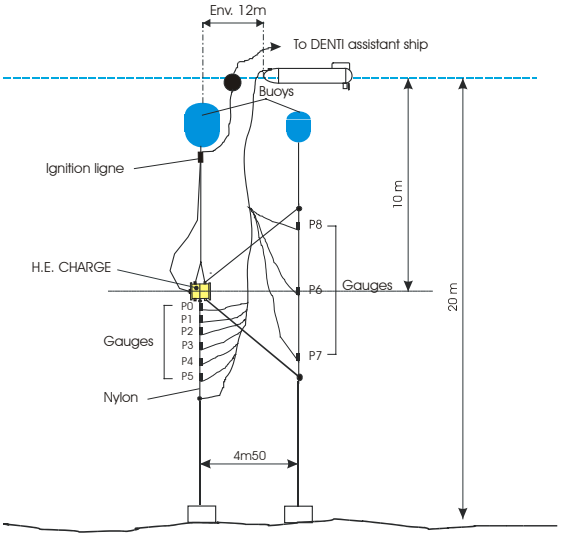

FIGURE 11 - GENERIC UNDEX EXPERIMENTAL SET-UP

Experimental results

The standard parameters of an underwater explosion are derived from pressure history measurements : Peak pressure P_{max}, the time constant θ, Impulse I for the shock wave and the pseudo-period T for the gas bubble (time to undergo a complete cycle "initial radius – expansion – maximum radius – collapse").
Experimental values for G111N and G111L are compared to two standard explosives TNT and HBX1, whose similitude coefficients are taken from Swisdak[16]. The peak pressure and impulse versus scaled distance are shown respectively figure 12, and the pseudo-period is presented table 4.

The composition G111L without aluminum shows similar impulse as TNT, but a decrease of the peak pressure and of the pseudo-period.

The composition G111N with nanometric aluminum shows a significant increase of the impulse about 60% more than TNT, and a longer bubble period 18% more than TNT and +4% for HBX1, although the peak pressure is similar to TNT results.

These similar result on peak pressure values indicates that the G111N higher impulse and the bubble effects are subsequent to a late energy release induced by aluminum burning mechanism.
Unfortunately, comparisons with G111M have not been possible. However, results available for other compositions of that kind do not show such increase of impulse and bubble effects.

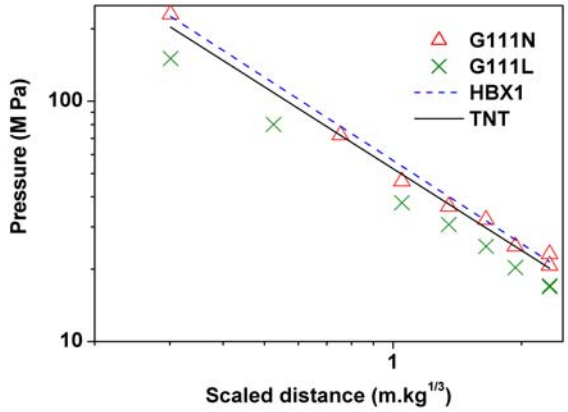

FIGURE 12 - PEAK PRESSURE VERSUS SCALED DISTANCE

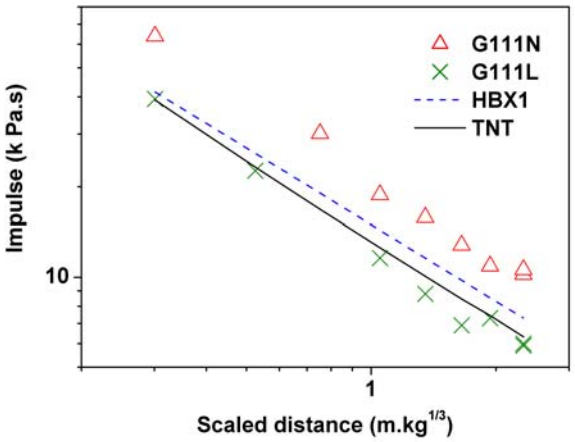

FIGURE 13 - IMPULSE VERSUS SCALED DISTANCE

TABLE 4 - BUBBLE PSEUDO PERIOD DURATION

	TNT	TNT	HBX1	G111N	G111L
Mass (kg)	12.55	20.7	12.55	12.55	12.55
T (ms)	406	479	463	479	376

DISCUSSION AND CONCLUSION

Both experiments and simulations concerning propagation of detonation inside RDX-AP-Al-wax HE show that a decreasing in aluminum particles diameter doesn't change significantly the D_n-κ characteristic. Slightly variations are observed for only G258 HE which trend is to diminish the detonation velocity. However, a non negligible initial fraction of Al_2O_3 is present at the surface of nanometric aluminum particles: a 3 nm Al_2O_3 thickness led to a 18.7% weight contents for G111N and 9.0% for G258N. Thermochemical simulations highlight a decreasing in detonation velocity of about 500 m/s and 120 m/s for G111N and G258N. Comparison between experimental and calculated D_n-κ using both Cheetah 2.0 thermochemical code and a 2-phases hydrocode led to conclude that improvements in modeling will be necessary.

Nanometric aluminum additive in RDX-AP-Al-wax HE slightly decreases their ballistics for high RDX weight percent and has no influence for lower RDX weight percent. We also expect that this behavior is mainly due to the presence of initial alumina layer at the surface of the particles.

DP emission spectra have been extensively studied to determine the DP thermo-optic characteristics and their temperature. Heat conduction at the interface LiF-RP and radiation transfer inside RP has been studied prior emission spectra analysis and determination of temperature. Higher temperatures are obtained for "Alex" nano-particles based compositions with a gap of ~ 1000 K for G111 HE and ~ 100 K for G258 HE comparing to 5μm Al. In an other hand, our results seem to highlight a very low volume fraction of carbon in G111 DP and we expect that temperatures obtained for this HE are probably aluminum temperature. It is not so clear for G258 HE: the temperature of DP containing nano-scale Al particles seems to be the gas temperature whereas we can not conclude for 5 μm particle diameter. These results are in favor of thermal non-equilibrium aluminum-gas phase mix with a difference of ~1500 K for G258M HE.

Blast and underwater effects have been evaluated only for the compositions G111. It is surprising that the composition G111N with nanometric aluminum gives reflected blast parameters higher than the composition G111M, 82% in reflected pressure and 16 % in reflected impulse, although the side-on pressure and impulse are similar. G111N shows also a significant increase of the underwater impulse about 60% more than TNT, and a longer bubble period 18% more than TNT and +4% for HBX1, although the peak pressure is similar to TNT results.

These results seems to be associated to high aluminum temperature and thermal non-equilibrium of the gas-particles mix, and highlight the importance of thermal transfer between hot aluminum (and/or alumina) particles and the gaseous DP. Metallic additive combustion lead to hot particles in which a large part of energy released by oxidation is stored. The transfer of this energy toward the gaseous phase by conduction and convection heat transfer is a long time phenomenon which can occurs during a few 100 μs up to a few ms. It can considerably modify the gas thermodynamics, acoustic waves and thus, the blast and underwater effects at long distance.

This study highlights that thermal characteristics, reflected blast and underwater effects would be the potential interest of reducing aluminum additive to nano-scale inside highly non-ideal HE. Continuation of this work would consist of a more systematic study of aluminized HE oxygen balance effects on thermal characteristics, blast parameters, internal blast and underwater effects. Temperature measurements would be improved using both time and wavelength resolved emission spectroscopy.

REFERENCES

1. Baudin G, Lefrançois A., D. Bergues, J. Bigot, Y. Champion, "Combustion of nanophase aluminum in the detonation products of nitromethane and TNT", 11th symposium on Detonation, 1998.

2. Sedoi V.S., Valevich V.V. et al., "Electroexplosive powders: production, physico-chemical properties and reactivity", Tomsk, 1999, private communication.

3. Ivanov J.Y., Tepper F., "Activated aluminum as a stored energy source for propellants", Challenges in Propellants and Combustion, edited by Kenneth K. Kuo, 1998.

4. Lefrançois A., Le Gallic C, Baudin G., "Nanometric aluminum powder influence on the detonation efficiency of high explosives", ICT, Fraunhofer Institute Conference, July 03-06, 2001.

5. Miller P.J., Beford C.D., Davis J.J., "Effect of metal particle size on the detonation properties of various metallized explosives", 11th Symposium on Detonation, Snowmass village, Colorado, 1998.

6. Stewart D.S and Bdzil J.B., "A lecture on detonation-shock-dynamics", US/Japan Workshop on Combustion, 1987.

7. Wood W.W. and Kirkwood J.G., "Diameter effect in condensed explosives: the relation between velocity and radius of curvature in the detonation wave", J. Chem. Phys. 22, 1920-1928, 1954.

8. Fried L.E., Howard W.M., Souers P.C., "Cheetah 2.0 User's Manual, UCRL-MA-117541, Rev. 5, august 20, 1998.

9. Chinnayya A., Daniel E., Saurel R., Baudin G., "A new concept for the modeling of detonation waves in multiphase mixtures", in this same Symposium.

10. B. Leal-Crouzet, R. Bouriannes, G. Baudin, J.C. Goutelle, "Ultrafast optical pyrometry for the measurements of detonating explosive temperatures", Eur. Phys. J. AP, 8 (1999), 189-194.

11. B. Leal, Baudin G., Goutelle J.C., Presles H.N., "An optical pyrometer for time resolved temperature measurements in detonation wave", 11th International Symposium on Detonation, Snowmass village, Colorado, 1998.

12. Le Gallic C., Serradeill R., "Anomalous emission of LiF crystal submitted to plane shock impact", private communication, 2002.

13. M.F. Modest, "Radiative heat transfer", Mc Graw-Hill International Editions 1993.

14. Baillis D., Sacadura J.F., "Thermal radiation properties of dispersed media: theoretical prediction and experimental characterization", Journal of Quantitative Spectroscopy & Radiative Transfer, 67, 327-363, 2000.

15. Winter N.W., Ree F.H., "Stability of the graphite and diamond phases of finite carbon clusters, 11th Symposium on Detonation, 1998.

16. Swisdak M.M., NSWC/NOL, Technical Report 76-116